

Density Measurement and Atomic Structure Simulation of Metastable Liquid Ti-Ni Alloys



P.F. ZOU, H.P. WANG, S.J. YANG, L. HU, and B. WEI

The temperature dependence of the densities of liquid Ti-Ni alloys was investigated by the electrostatic levitation technique and molecular dynamics simulation. The average cooling rate by natural radiation decreases with a reduction in Ti content and reaches its minimum at $\text{Ti}_{55}\text{Ni}_{45}$ alloy. The Ti-Ni alloy system exhibits a negative excess volume and it becomes smaller with the increase in undercooling. This indicates that the interactions among atoms are enhanced with the decrease in temperature. The pair correlation functions and static structure factors are obtained from the molecular dynamics results. It is found that the packing of the Ni atoms does not occur through replacement of the Ti atoms with the addition of Ni atoms. In addition, the clusters are abundant in liquid Ti-Ni alloys, and a tetragonal bipyramid atomic configuration of may exist. It is found that the Ni-Ni bonds transform to Ti-Ni bonds with the increase in Ni content.

<https://doi.org/10.1007/s11661-018-4877-8>

© The Minerals, Metals & Materials Society and ASM International 2018

I. INTRODUCTION

TO assure that metallic materials can be applied in extreme environments and improved performance, the metal in its liquid state is an important aspect that should be considered. The prime question being put forward is the difference in the thermophysical properties between the solid and liquid states for the same metal. Since the high activity of liquid metals would result in reactions with the container under high-temperature conditions, the traditional methods adopted to measure the properties of solid metals are not suitable for liquid metals. Thus, novel measurement methods including containerless techniques such as electrostatic levitation (ESL), electromagnetic levitation (EML), and aerodynamic levitation^[1-3] are developed.

Thermophysical properties, such as density, thermal expansion, heat capacity, surface tension, and viscosity,^[4-7] have been measured by levitation methods. Density is one of the most fundamental properties of materials; it is a critical parameter for metallurgical processing, casting simulation, heat transition calculation, surface tension, and viscosity determination. While the liquid structure is related to the thermophysical properties, scientists further study the packing of atoms and clusters in liquid alloys by combining the levitation technique with synchrotron radiation.^[8,9] At the same

time, computational simulations are rapidly developed; these are good choices to observe the arrangements of atoms. Using the reverse Monte Carlo, molecular dynamics (MD), and first-principle simulations, investigations of the thermophysical properties and structural information of liquid alloys have been reported, such as for the binary alloy systems Zr-Ni, Al-Au, Fe-Cu, Al-Cu, and Al-Ni.^[10-13] Peng *et al.*^[12] measured the densities and viscosities of liquid Al-Au alloys by EML, which agreed with the results achieved from MD simulation. Ding *et al.*^[14] used the MD method to simulate two metallic glass-forming systems. They found that the excess specific heat would increase with the increasing development of structural ordering.

The Ti-Ni binary alloy system consists of intermetallic compounds, eutectic alloys, and solid solutions. The $\text{Ti}_{50}\text{Ni}_{50}$ alloy is the most famous alloy in Ti-Ni alloy system due to its excellent shape memory effect, good biocompatibility, and mechanical properties,^[15-17] which have been studied extensively. In addition, the mechanism of martensitic transformation has attracted much attention.^[18,19] To improve the properties and broaden the range of application, research on adding extra elements based on the Ti-Ni alloy is also popular.^[20,21] For other Ti-Ni alloys, the work focuses on their glass-forming ability,^[22-24] while the final performance is directly related to the solidification process in which the alloy transforms from the liquid to solid state. Thus, the studies on the thermophysical properties and structure of liquid alloys are indeed important and necessary. If the understanding of liquid metals is deep enough, the theory of liquid alloys could be established, and the desired materials could be obtained. However, studies of the thermophysical

P.F. ZOU, H.P. WANG, S.J. YANG, L. HU, and B. WEI are with the Department of Applied Physics, Northwestern Polytechnical University, Xi'an 710072, P. R. China. Contact e-mail: hpwang@nwpu.edu.cn

Manuscript submitted February 20, 2018.

Article published online August 13, 2018

properties and the packing of atoms in the liquid state are rare. Because the activities of liquid Ti-Ni alloys are very high, the sample would be polluted if the liquid Ti-Ni alloy is held in a container. Using the ESL technique, the sample does not contact with the container, and it is convenient to obtain the thermophysical properties by combining various detectors. While neutron diffraction and synchrotron radiation are effective ways to investigate the liquid structure, these opportunities are rare, and the detailed research is extremely limited. For this reason, it is suitable to simulate the liquid structure by means of MD simulation.

In this paper, the densities of liquid Ti-Ni alloys were measured by ESL and compared with the results obtained by MD simulation. Meanwhile, the molar volume and excess volume are discussed. The pair correlation function $g(r)$ and structure factor $S(q)$ are analyzed to gain information about the atomic structure of liquid Ti-Ni alloys.

II. METHODS

A. Electrostatic Levitation Experiment

For the Ti-Ni alloys, the molar fractions of Ni distributed in 0, 10, 20, 24, 40, 45, 50, 55, 61, 83.5, and 100 pct alloys were chosen to investigate the relationship between the Ni content and the liquid density. The first step was to obtain the master alloys, which were prepared from 99.999 pct Ni and 99.999 pct Ti with a deviation less than 0.1 pct. These were then melted under an Ar atmosphere in an arc melting furnace. Subsequently, to ensure the acquisition of accurate densities in the liquid state, the master alloys were separated into several portions, which would later be remelted to spheres using a laser.

An illustration of the density measurement system is shown in Figure 1. The sample was levitated between vertical electrodes coupled with four-side electrodes in a chamber that could be evaluated to 10^{-5} Pa. Before the levitation process, sample preheating was necessary to ensure that the sample charge was sufficient. When the sample was steadily levitated, it was heated to the liquid state by an SPI SP300 fiber laser with a wavelength of 1070 nm. The sample temperature was measured by a

single-color PA-40 pyrometer ranging from 850 to 3000 K. The emissivity calibration at the liquidus temperature (T_L) plateau was maintained all the time since the emissivity only slightly changed during the experiment. Additional information about our ESL facility has been reported elsewhere.^[25]

With the help of UV background light, a CMOS camera with a resolution of 700×700 pixels recorded the photographs of the liquid sample with a recognizable edge in a wide temperature range, as shown in Figure 1(b). The shape of the sample is rotationally symmetric to the vertical axis, as marked in Figure 1(b). The edge could be gained by the grayscale process and fitted with the sixth-order Legendre polynomial. Then, the volume of the liquid sample could be obtained by the integration of the Legendre polynomial. The volume is calculated as follows:

$$R(\theta) = \sum_{i=0}^6 a_i P_i[\cos(\theta)] \quad [1]$$

$$V = \frac{2}{3} \pi q^3 \int_0^\pi R(\theta)^3 \sin(\theta) d\theta, \quad [2]$$

where $P_i[\cos(\theta)]$ is the i th-order Legendre polynomial and a_i is the corresponding coefficient. $R(\theta)$ is the edge function of the rotation angle of θ . The calibration factor q represents the length of a pixel corresponding to the real length, which is determined by a steel ball with a certain density. The mass of the samples could be weighted after experiments, and the value could be considered the mass during experiment because the mass loss is extremely small. Then the liquid density of the sample is determined by the following equation:

$$\rho = \frac{m}{V}. \quad [3]$$

B. Molecular Dynamics Simulation

In addition to the experiments, the MD simulation is performed to obtain the liquid densities and further information about the liquid structure. The potential

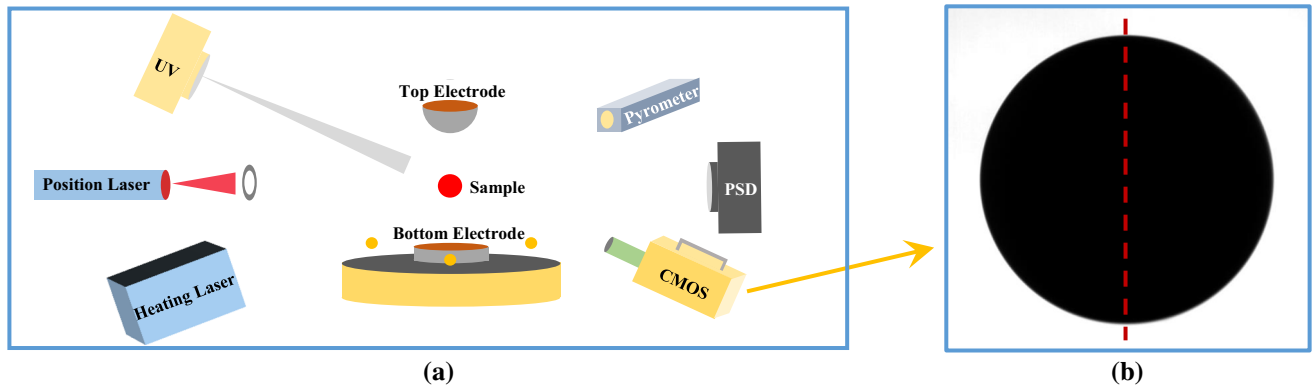


Fig. 1—The schematics of density measurement: (a) the illustration of electrostatic levitation system; (b) the image of liquid sample recorded by CMOS camera.

function used for simulation is the modified embedded-atom method (MEAM) model, which has been successfully applied to various binary and ternary alloys. It is defined by^[26]

$$E = \sum_l \left[F_i(\bar{\rho}_i) + \frac{1}{2} \sum_{j \neq i} S_{ij} \phi_{ij}(R_{ij}) \right], \quad [4]$$

where F_i is the embedding energy related to the electron density $\bar{\rho}_i$, R_{ij} and ϕ_{ij} are the distance and pair interaction between two different atoms i and j . S_{ij} is the screening function, which is adjusted by Baskes to solve some problems caused by previous S_{ij} . More recently, Won-Seok Ko *et al.*^[27] developed a MEAM potential for Ti-Ni binary alloys to describe the martensitic B2-B19' transition in Ti-Ni shape memory alloy. In this paper, the MEAM potential was used to calculate the densities and the structure factors of Ti-Ni alloys in the liquid state.

For the MD simulation of Ti-Ni system alloys, the compositions with Ni contents of 0, 10, 20, 24, 40, 45, 55, 61, 83.5, and 100 pct are selected. In the beginning, 8000 atoms coupled with Ti and Ni atoms were arranged in a cubic box with periodic boundary conditions. The NPT ensemble was adopted to simulate the actual environment. The time step was set to 1 fs, and the pressure was set to 1 bar. To guarantee that the system would be in the liquid state, the initial temperature was set to 3000 K. The system was run under the initial temperature for 200,000 steps to produce a homogenous distribution of the atoms. Then, the system was cooled 100 K with a cooling rate of 10^{12} K s⁻¹. At each temperature plateau, 100,000 steps would be used to balance the system, and the data were collected in the following 50,000 steps with an interval of 50 steps. All the scripts were run by LAMMPS on Lenovo servers.^[28]

After the simulation, the volume data were extracted from the output file, and the density could be derived as a combination of the mass of atoms. Apart from the thermophysical properties, the structural information could also be obtained from the MD simulation. The pair correlation function ($g(r)$) is a good approach to reflect the arrangements among atoms and is defined by the following:

$$g_{ij}(r) = \frac{V}{N_i N_j} \left\langle \sum_{i=1}^{N_i} \frac{n_{ij}(r, \Delta r)}{4\pi r^2 \Delta r} \right\rangle, \quad [5]$$

where g_{ij} is the partial pair correlation function between the i - j bond. V is the volume of a supercell, N_i and N_j represents the numbers of icons of the i th and j th type of atom, and $n_{ij}(r, \Delta r)$ is the number of the j th type of atom at the range from r to $r + \Delta r$. The angular brackets indicate the time average. The MD simulation could output the coordinates of all atoms for each step. Thus, $g(r)$ could be derived by programing and digitally analyzing the location file.

III. RESULTS AND DISCUSSION

The typical cooling curves of the liquid Ti-Ni alloys are shown in Figure 2. An entire cooling curve containing the heating and cooling process is presented in Figure 2(j). At the moment that the alloy is heated to its liquidus temperature, a temperature plateau will remain for seconds until the alloy is completely melted. Then, the emissivity is calibrated. When the temperature of the sample exceeded T_L and remained for a moment to ensure that the melt was homogeneous, the laser was shut down. The sample would be cooled by free radiation and the average cooling rates are marked in

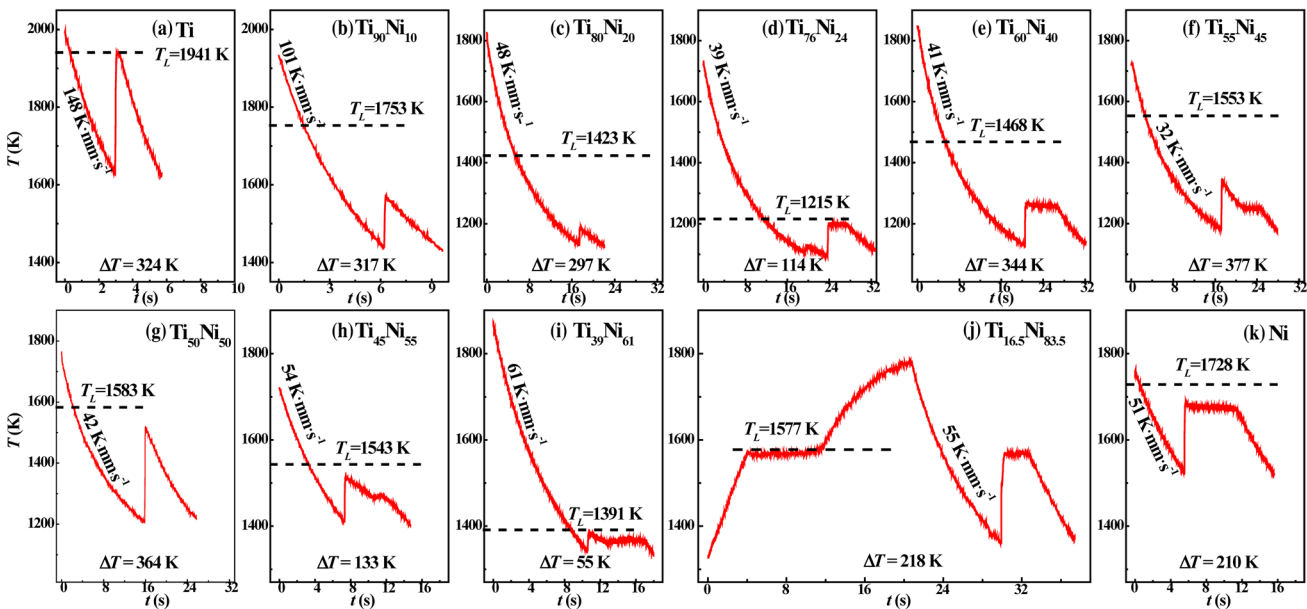


Fig. 2—Typical cooling curves of liquid Ti-Ni alloys: (a) Ti; (b) Ti₉₀Ni₁₀; (c) Ti₈₀Ni₂₀; (d) Ti₇₆Ni₂₄; (e) Ti₆₀Ni₄₀; (f) Ti₅₅Ni₄₅; (g) Ti₅₀Ni₅₀; (h) Ti₄₅Ni₅₅; (i) Ti₃₉Ni₆₁; (j) the entire time-temperature profile of Ti_{16.5}Ni_{83.5}; (k) Ni.

Figure 2, respectively. The radii of the Ti-Ni samples in the liquid state are in a range of 1.17 to 1.22 mm. While the cooling rate in a vacuum environment is inversely proportional to the radius, a reduced cooling rate (R_r) is defined for comparing the cooling rates of different metals and alloys. It is described as follows:

$$R_r = R_c \cdot r, \quad [6]$$

where R_c is the average cooling rate and r is the radius of the sample. The results show that the liquid Ti could transfer heat to the surrounding environment faster than the liquid Ni. For the Ti-rich part of the alloys, the reduced cooling rates decrease rapidly with the decrease in Ti content. This may result from the lower melting temperature, which results in the diverse temperature ranges during density measurement, while the average cooling rate shows biquadratic growth with the increase in the upper limit of the measured temperature. For the compositions with Ni contents close to the Ti content, the reduced cooling rates are lower, and the minimum rate occurs at $T_{i55}Ni_{45}$. In contrast, the rates increase slightly with the decrease in Ti content in the Ni-rich section.

When the temperature decreases to somewhere lower than the liquidus temperature, the recalescence phenomenon occurs. This is exhibited in Figure 2 as an abrupt rise in temperature. The solidification types are abundant in the chosen Ti-Ni alloys. For the $Ti_{55}Ni_{45}$ alloy, there are an exothermic peak and a plateau on the cooling curve, which correspond to the formation of the primary TiNi and peritectic Ti_2Ni phase, respectively. The maximum undercooling ΔT is 377 K, which reaches $0.24T_L$, as shown in Figure 2(f). Furthermore, the liquid $Ti_{50}Ni_{50}$ alloy directly solidifies to the intermetallic compound TiNi phase with undercooling to 364 K ($0.23T_L$), as seen in Figure 2(g). When the $Ti_{16.5}Ni_{83.5}$ alloy is undercooled to 218 K, the recalescence occurs with a formation of eutectic consisted of Ti_3Ni and Ni phase, as seen in Figure 2(j). It is noted that large undercoolings are achieved for most Ti-Ni alloys. The large undercooling promises a wider range for the

measurement of liquid thermophysical properties and provides help for the understanding of solidification from the metastable liquid.

When the mass of the sample after experiment is obtained, the density could be derived by combining the volume in the liquid state calculated from the recorded images. The measured densities of the investigated 11 compositions of Ti-Ni alloys are displayed in Figure 3(a). It is found that the liquid density increases with the decrease in temperature for all alloys. Apart from the quadratic density dependence on temperature of the $Ti_{50}Ni_{50}$ alloy,^[25] the densities of other liquid Ti-Ni alloys all exhibit linear relationships with temperature. In addition, the density increases with the increase in the molar fraction of Ni. The linear relationship could be expressed by

$$\rho = \rho_L + \frac{\partial \rho}{\partial T}(T - T_L), \quad [7]$$

where ρ_L and $\partial \rho / \partial T$ are the density at the liquidus temperature and the temperature coefficient.

The density measurement uncertainty mainly results from the mass, volume, and temperature measurements. The uncertainty could be evaluated by the following equation:^[29]

$$(\Delta \rho)^2 = \left(\frac{\partial \rho}{\partial m} \Delta m \right)^2 + \left(\frac{\partial \rho}{\partial V} \Delta V \right)^2 + \left(\frac{\partial \rho}{\partial T} \Delta T \right)^2 \quad [8]$$

$$\left(\frac{\Delta \rho}{\rho} \right)^2 = \left(\frac{\Delta m}{m} \right)^2 + \left(\frac{\Delta V}{V} \right)^2 + \left(\frac{\Delta T}{T} \right)^2. \quad [9]$$

Usually, the samples used for density measurements weigh approximately 30 mg, and the mass loss is not more than 0.03 mg after experiments for Ti-Ni alloys. The uncertainty of volume measurement is mostly a consequence of the calibration factor and the difference between the pixel volume and real volume. The error of the calibration factor is ± 0.42 pct through the steel ball with certain density. The other error is obtained by

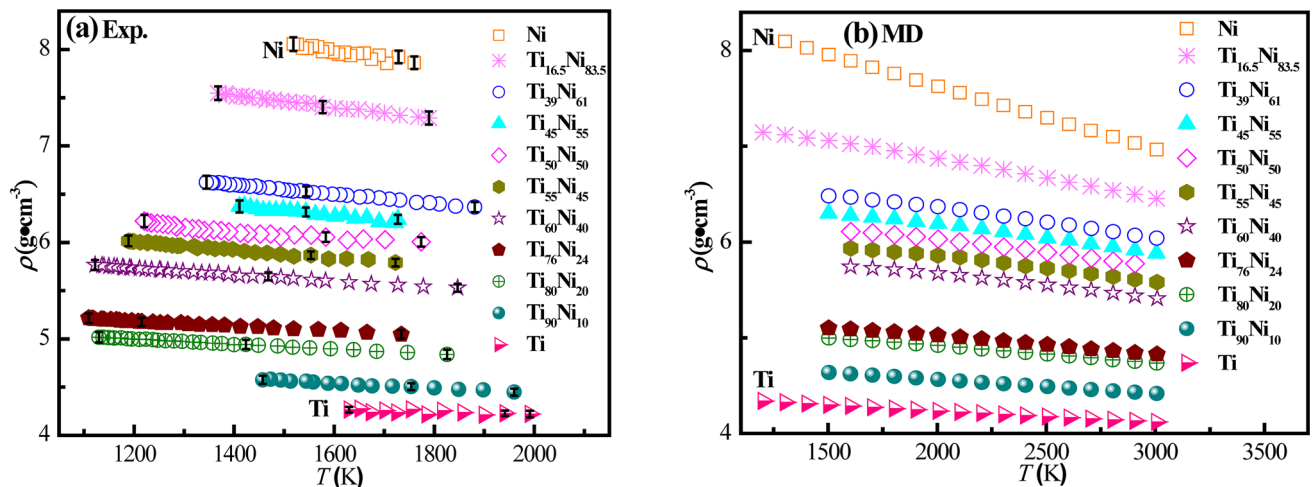


Fig. 3—Liquid densities of eleven Ti-Ni alloys vs temperature: (a) electrostatic levitation measurement; (b) molecular dynamics simulation.

calculating the volumes from 2000 images at the same temperature. The uncertainty of the pixel for Ni at its T_L is ± 0.54 pct, and thus, the total uncertainty of volume is ± 0.68 pct. Considering that the accuracy of the pyrometer and the emission of the melt change with temperature, the temperature uncertainty for Ni is evaluated to 0.2 pct. The density measurement uncertainty for Ni at its T_L is 0.83 pct, as seen in Figure 3(a). The uncertainty varies with temperature, so the uncertainties at its lower and upper temperature limits are also presented in Figure 3(a). The uncertainties at the entire temperature range are between the values marked in the density curves.

In addition to the ESL experiments, the MD simulations were used to calculate the liquid densities of the Ti-Ni alloys, as shown in Figure 3(b). It is seen that the liquid densities increase linearly as the temperature decreases, and the densities increase with increasing Ni content, which is in agreement with the experimental results. For the composition of the Ti₅₀Ni₅₀ alloy, the difference in the densities at T_L between the experiment and calculation is 1.5 pct. In contrast, the density derived from MD simulation shows a linear relationship with temperature, which is different from the result measured by the ESL experiment. A possible reason for this is that the potential function may not match the Ti₅₀Ni₅₀ alloy well so that it could not completely reflect the actual situation.

The values of the liquid densities at T_L and the temperature coefficients obtained from the two methods are listed in Table I. It can be seen that the liquid density of pure Ni experimentally measured at T_L is 7.89 g cm⁻³, while the simulation result is 7.80 g cm⁻³. Compared to the result of 7.89 g cm⁻³ measured by Ishikawa *et al.*,^[30] the experimental value is in good agreement, and the simulation value reported in this work is different by 1.1 pct. Yoo *et al.*^[29] also measured the liquid density of Ni by electrostatic levitation, and the value at T_L is 7.79 g cm⁻³, which differs by 1.3 and 0.1 pct from the experimental and simulant results. For

pure Ti, the experimental and simulation values are 4.22 and 4.25 g cm⁻³, respectively, while the value measured by Paradis *et al.* is 4.21 g cm⁻³,^[31] which agrees well with our results. For other Ti-Ni alloys, the liquid density data have not been reported by others. The differences in the liquid density at T_L between the experimental and simulation values are within 6 pct for all compositions, and most of them are less than 2 pct. As a result, it is believed that the experimental data are accurate and the simulation results are reliable.

In the case that the liquid density of a certain alloy at a specific temperature is needed but the data are absent and only the data of the corresponding pure metals are available, the liquid alloy is treated as an ideal solution. The linear interpolation method is adopted to obtain the density value. It is considered that no interaction among atoms exists in an ideal solution, but in fact, attractive or repulsive forces exist between two different types of atoms; therefore, the density and molar volume generally would not obey the law of ideal solutions. The liquidus temperatures and temperature measurement ranges of Ti-Ni alloys are different with compositions, so the practical molar volumes vs Ni content at $T = 1700, 1500, \text{ and } 1300$ K are shown in Figure 4. The molar volume decreases as the Ni content increases, and the values are all lower than the values obtained from linear extrapolation. The molar volumes derived from experiments and simulations at 1700 K are both illustrated in Figure 4(a). The molar volume obtained from MD simulation decreases with increasing Ni content. The differences between the two methods are all within 0.4 cm³ mol⁻¹, which is approximately 5 pct deviation.

To further judge the degree of mixture of the Ti-Ni alloys, the excess volume V_E is necessary, which is defined as

$$V_E = V_M - \sum_i c_i V_i, \quad [10]$$

Table I. The Densities of Liquid Ti-Ni Alloys Obtained from Electrostatic Levitation Experiments and Molecular Dynamic Simulations

Alloy	T_L (K)	ESL Experiment				MD Simulation			
		ρ_L (g cm ⁻³)	$\partial\rho/\partial T$ (10 ⁻⁴ g cm ⁻³ K ⁻¹)	$\partial^2\rho/\partial T^2$ (10 ⁻⁷ g cm ⁻³ K ⁻²)	Temperature Range (K)	Density Error at T_L (g cm ⁻³)	ρ_L (g cm ⁻³)	$\partial\rho/\partial T$ (10 ⁻⁴ g cm ⁻³ K ⁻¹)	Temperature Range (K)
Ti	1941	4.22	- 1.69	0	1617-1991	0.0279	4.25	- 1.21	1200-3000
Ti ₉₀ Ni ₁₀	1753	4.50	- 2.46	0	1436-1959	0.0362	4.60	- 1.48	1500-3000
Ti ₈₀ Ni ₂₀	1423	4.94	- 2.64	0	1126-1825	0.0473	5.02	- 1.78	1500-3000
Ti ₇₆ Ni ₂₄	1215	5.10	- 2.60	0	1101-1734	0.0436	5.16	- 1.88	1500-3000
Ti ₆₀ Ni ₄₀	1468	5.64	- 3.42	0	1122-1847	0.0410	5.79	- 2.41	1600-3000
Ti ₅₅ Ni ₄₅	1553	5.86	- 4.20	0	1176-1722	0.0400	5.97	- 2.59	1600-3000
Ti ₅₀ Ni ₅₀	1583	6.04	- 2.34	6.52	1219-1774	0.0487	6.13	- 2.66	1600-3000
Ti ₄₅ Ni ₅₅	1543	6.30	- 4.68	0	1408-1727	0.0463	6.31	- 2.81	1500-3000
Ti ₃₉ Ni ₆₁	1391	6.60	- 4.84	0	1336-1880	0.0521	6.54	- 3.02	1500-3000
Ti _{16.5} Ni _{83.5}	1577	7.42	- 6.09	0	1359-1779	0.0634	7.03	- 3.90	1200-3000
Ni	1728	7.89	- 6.83	0	1511-1760	0.0671	7.80	- 6.61	1300-3000

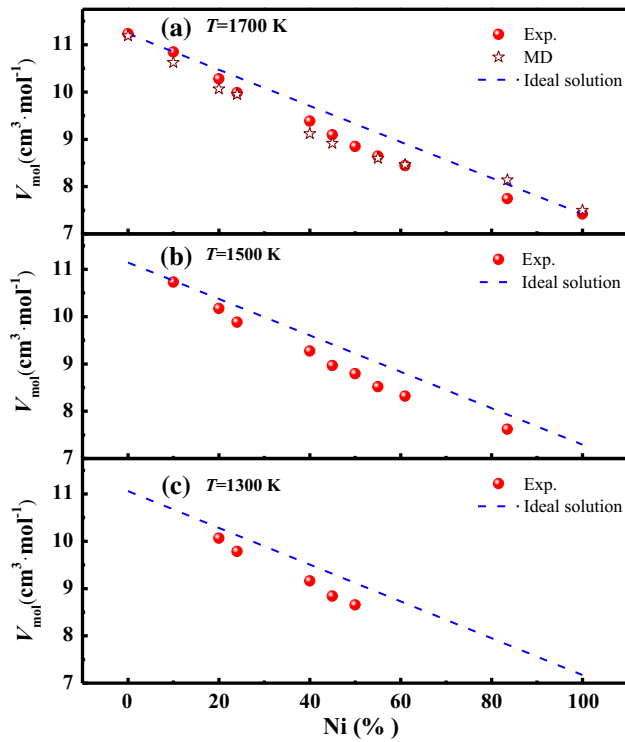


Fig. 4—Molar volume of liquid Ti-Ni alloys at different temperatures: (a) $T = 1700$ K; (b) $T = 1500$ K; (c) $T = 1300$ K.

where V_M is the molar volume of alloy, c_i and V_i represent the atomic fraction, and molar volume of the i th component. The excess volumes derived from experiments vs the Ni content are shown in Figure 5, which exhibits negative values for each temperature. The excess volume is available partly at lower temperatures because the undercooled melt could not reach a lower temperature for some alloys. At 1700 K, the excess volume decreases first and reaches a minimum when the Ni content increases to 55 pct. Then, the excess volume increases with increasing of Ni content, which indicates that the liquid $Ti_{45}Ni_{55}$ alloy is the most miscible of the Ti-Ni alloys. It can be easily observed that the excess volumes of the Ti-Ni alloys decrease slightly as the temperature changes from 1700 to 1500 K and finally decreases to 1300 K, except for the $Ti_{50}Ni_{50}$ alloy, for which the excess volume achieves its minimum at 1700 K and the value at 1300 K is smaller than that at 1500 K, as shown in the ellipse in Figure 5. The excess volume could reflect the degree of mixture between different types of atoms. If the excess volume is positive, it is possible for the phase separation to occur. For most alloys, the excess volumes are negative, which suggest that they are miscible. If the excess volume deviates more seriously when compared to the excess volume of an ideal solution, the attraction force among atoms would be stronger. This is to say that the bond pairs strengthen with the decrease in temperature for Ti-Ni alloys.

The various liquid densities of Ti-Ni alloys are determined by both the different molar masses and the changes in volumes, in which the volumes play an

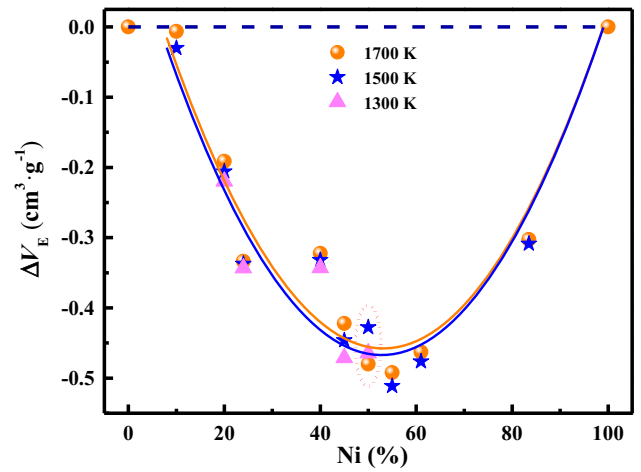


Fig. 5—Measured excess volumes vs Ni composition at different temperatures.

important role. For Ti-Ni alloys, it shows a strong negative excess volume as seen in Figure 5. The structure and the atom arrangement lead to the strong negative excess volume. The $g(r)$ is an effective way to obtain structural information about the short-range ordering and is obtained from the MD simulation. In Figure 6, the total and partial pair correlation functions are shown. The position of the first peak of $g_{total}(r)$ shifts to the low- r side with the addition of Ni content, changing from 2.78 Å of Ti to 2.44 Å of Ni. Apart from the nearest-neighbor peak position, the position of secondary and higher-order peaks also shifts to the low- r side with an increase of Ni content. In addition, the intensity of $g_{total}(r)$ at the nearest-neighbor peak increases slightly when the Ni content changes from 10 to 83.5 pct, indicating that the ordering increases in liquid alloys when the composition changes. For the partial $g_{Ti-Ti}(r)$ in Figure 6(c), the shapes of the pair correlation functions at different Ni concentrations are similar. This indicates that the Ti-Ti bonds in the Ti-Ni alloys do not change much. A study of the structural parameters of amorphous $Ni_{60}Ti_{40}$ alloy measured by Extended X-ray absorption fine structure (EXAFS) method shows that the distances between Ni-Ni, Ti-Ni, and Ti-Ti pairs are 2.49, 2.54, and 2.88 Å, respectively.^[32] Compared to the adjacent component of the $Ti_{39}Ni_{61}$ alloy, the corresponding distances are 2.50, 2.56, and 2.88 Å, respectively. The simulation results fit the experimental values well.

A split at the secondary peak could be observed from $g_{total}(r)$, as seen in Figure 6(a). This is an indication that several clusters may exist. The $g_{total}(r)$ is the sum of the $g_{Ni-Ni}(r)$, $g_{Ti-Ti}(r)$ and $g_{Ti-Ni}(r)$, so the split of $g_{total}(r)$ at the secondary peak could be attributed to the split of $g_{Ni-Ni}(r)$ and $g_{Ti-Ni}(r)$ exhibited in Figures 6(b) and (d), and the split of $g_{Ni-Ni}(r)$ is the key. As shown in Figure 6(b), the position of the nearest-neighbor peak is at $r_{max} \approx 2.54$ Å, and the second peak splits into two peaks approximately 4.7 Å for $g_{Ni-Ni}(r)$. The inner and outer values of the secondary peaks are at 4.22 and 5.08 Å, corresponding to 1.66 r_{max} and 2.00 r_{max} ,

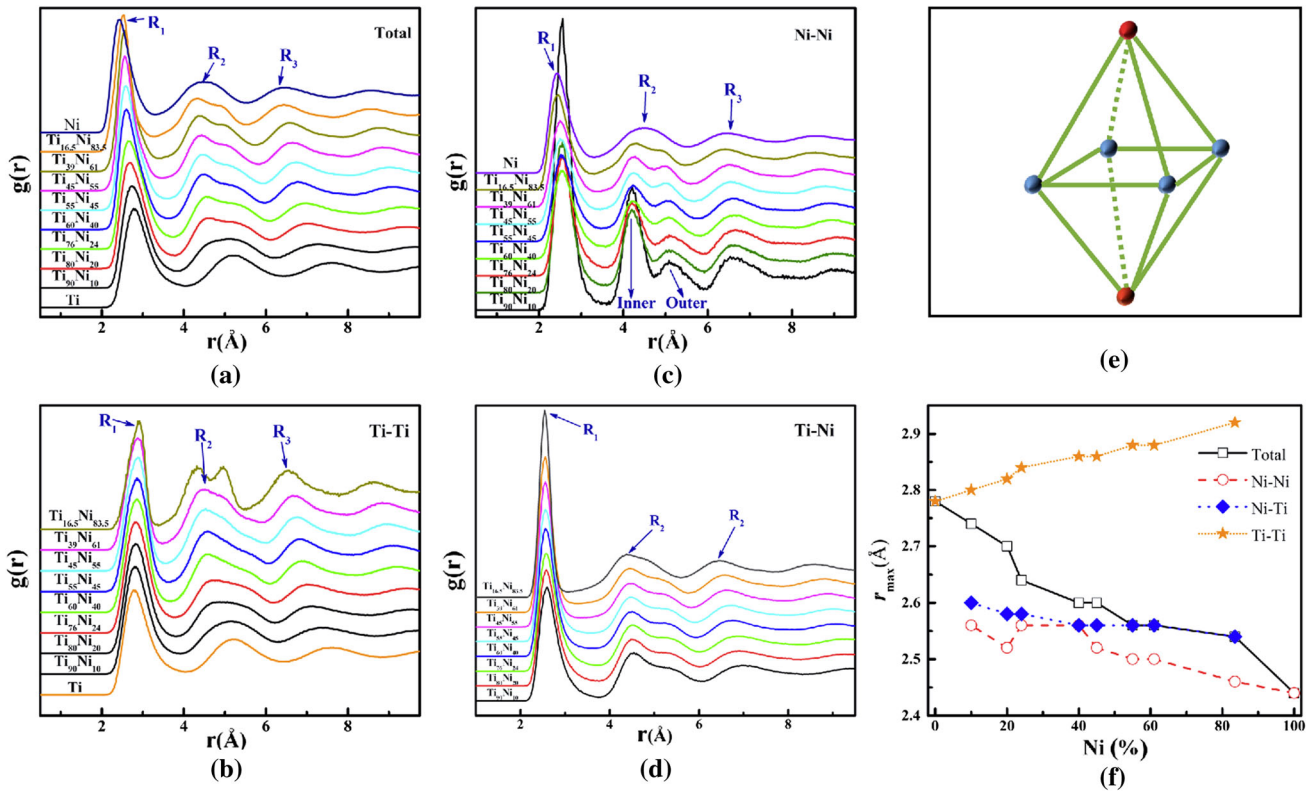


Fig. 6—Pair correlation functions of liquid Ti-Ni alloys at $T = 1700$ K: (a) the total pair correlation function; (b–d) corresponds to the Ti-Ti, Ni-Ni, Ti-Ni partial pair correlation functions, respectively; (e) the structure schematics of tetragonal bipyramid corresponding to the inner second peak; (f) the first-nearest peak position as a function of Ni concentration.

respectively. While for the tetragonal bipyramid, as Figure 6(e) shows, the distance between the atomic vertices is approximately $1.63 r_{\max}$, which matches the inner second peak position well. The $2.00 r_{\max}$ of the outer split at the second peak may correspond to a more complex cluster. Compared with the position at the second peak of pure Ni, it could be found that part of the Ni atoms pack more efficiently and another part of the Ni atoms have a more relaxed environment. With the addition of Ni content, the intensity of the inner second peak decreases gradually, suggesting that the ordering of the cluster corresponding to the inner split decreases with the increase in Ni content. In addition, the height of the first peak of $g_{\text{Ni-Ni}}(r)$ falls while the intensity of $g_{\text{Ti-Ni}}(r)$ increases at the first peak with more Ni content. This illustrates that the Ni-Ni bond transforms into Ti-Ni bond when the Ni concentration increases. On the other hand, the intensity of $g_{\text{Ni-Ni}}(r)$ at the first peak and inner second peak for the $\text{Ti}_{90}\text{Ni}_{10}$ alloy is far greater than that of other alloys while its Ni concentration is the lowest, which indicates that the Ni atoms have a strong self-aggregation effect when the Ni concentration is low.

To better evaluate the effect of Ni concentrations on the distances between different bonds, the relationship between the first-nearest peak position and Ni concentration is shown in Figure 6(f). The r_{\max} of $g_{\text{total}}(r)$ and $g_{\text{Ni-Ni}}(r)$ shifts to the low- r side with the increase in Ni content, which means that Ni atoms are packed more

densely, and thus, the volume of the liquid alloy would decrease with the increase in Ni content, corresponding to the decrease in molar volumes and the increase in densities. R_{\max} of $g_{\text{Ti-Ni}}(r)$ almost remains a constant. This suggests that the Ti-Ni bond is stable and insensitive to the Ni concentration. It is opposite to $g_{\text{Ti-Ti}}(r)$, for which r_{\max} shifts to the high- r side. It could be attributed to the Ti concentration decreasing with the addition of Ni. Although the volume is reduced, it cannot change the fact that the Ti atoms would be more sparsely distributed, resulting in the distance between Ti atoms becoming longer. It could be inferred that the Ni atoms are dominant in the liquid Ti-Ni alloys from the coordinating changes of the r_{\max} between $g_{\text{total}}(r)$ and $g_{\text{Ni-Ni}}(r)$. The Ni and Ti atoms do not pack through substitutional replacement, which is the packing way in liquid Au-Al alloys.^[12]

In addition to the pair correlation function, the $S(q)$ is also an important parameter that reflects the structural characteristics. The $S(q)$ could be obtained through the Fourier transform of $g(r)$, which is defined as

$$S(q) = 1 + 4\pi\rho \int_0^\infty (g(r) - 1) \frac{\sin(qr)}{q} dr, \quad [11]$$

where ρ is the average number density. $S(q)$ is shown in Figure 7. The static structure factors of pure Ni and Ti in the liquid state obtained from MD simulation are compared with the experimental results with adjacent

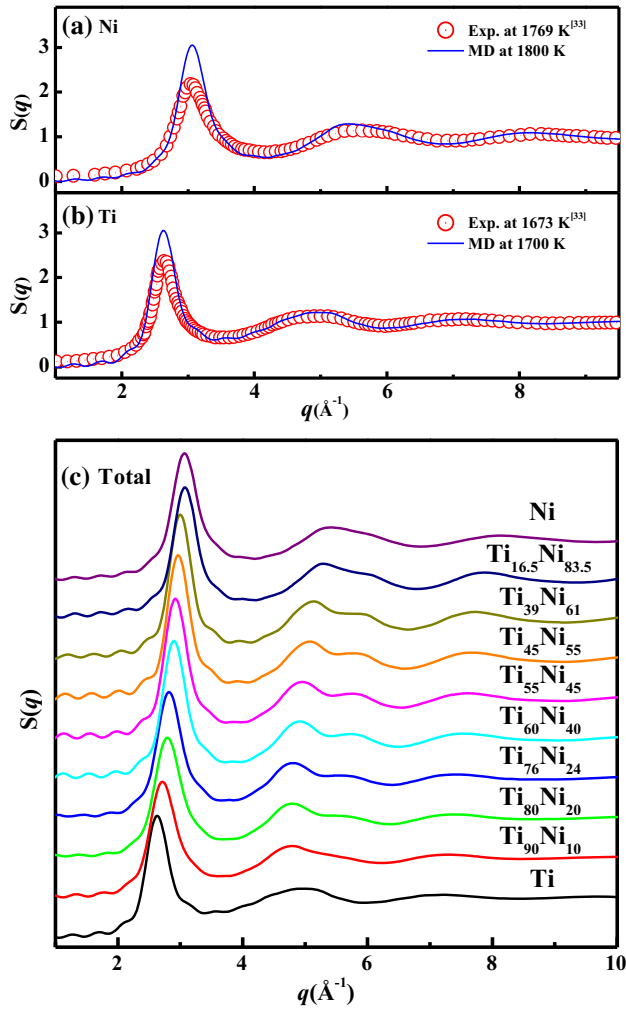


Fig. 7—The static structure factors: (a) the static structures of pure Ni in liquid state obtained from MD simulation and experiment which is adapted from Ref. [33]; (b) the static structures of pure Ti in liquid state obtained from MD simulation and experiment which is adapted from Ref. [33]; (c) the static structure factors of liquid Ti-Ni alloys at $T = 1700$ K.

temperatures, as shown in Figures 7(a) and (b).^[33] The agreements between the simulation and experimental results are good, which provides us great confidence in the results for other Ti-Ni alloys. There are a few fluctuations in the beginning because r is limited in the Fourier transform process. As shown in Figure 7(c), the wave vector q moves to the high- q side with the increase in Ni concentration, it corresponds to the decrease in the distance between atoms in practice and results in the increase in the liquid density. It is also noted that the second peak of $S(q)$ splits into a small peak and a shoulder for the Ti-Ni alloys with Ni concentrations from 20 to 61 pct. The shoulder at the second peak is usually identified as a signature of the icosahedral structure, while the icosahedral short-range order is considered a typical structure in metallic glass. For the Ti-Ni alloys, the alloys with Ni concentrations in the range from 12 to 82 pct have a higher glass-forming ability.^[24] As a result, the existence of icosahedral structure in liquid Ti-Ni alloys is possible.

IV. CONCLUSION

The high undercooling of liquid Ti-Ni alloys was realized under conditions of electrostatic levitation, where the maximum undercooling is 377 K ($0.24T_L$) within the liquid $Ti_{55}Ni_{45}$ alloy. By utilizing the CMOS camera, the liquid densities of 11 compositions were measured in the containerless state. Meanwhile, molecular dynamics simulation was adopted to calculate the densities of liquid Ti-Ni alloys. The agreement between the two methods is quite good. In addition, the molar volume and excess volume are obtained from the density result. In general, the liquid Ti-Ni alloys show a negative excess volume, which indicates that the Ti-Ni alloy system is miscible. With the decrease in temperature, the excess volume increases for most Ti-Ni alloys. On the other hand, the pair correlation functions were obtained from MD simulation. It was found that Ni atoms are more effective than Ti atoms in the liquid Ti-Ni alloys, and Ni atoms are dominant in the whole structure. In addition, the Ni-Ni bond shows a strong aggregation when the Ni concentration is low. With an increase in the Ni concentration, the Ni-Ni bonds transform into Ti-Ni bonds. The static structure factor was obtained from the Fourier transformation of $g(r)$. When compared with other Ti-Ni alloys or pure metals, there are some differences for $S(q)$ in the second peak for those Ti-Ni alloys whose Ni concentration is between 20 and 61 pct. It suggests that various clusters should exist with the different Ni concentrations.

ACKNOWLEDGMENTS

This work was financially supported by National Natural Science Foundation of China (Grant Nos. 51327901, 51522102, 51734008, and 51401169) and the Fundamental Research Funds for the Central Universities. The authors are grateful to Mr. P. Lü for helping in MD simulations, Miss L. Wang and Mr. C.H. Zheng for their help with the experiments.

REFERENCES

1. D.G. Quirinale, G.E. Rustan, A. Kreyssig, and A.I. Goldman: *Appl. Phys. Lett.*, 2015, vol. 106, pp. 241906–09.
2. R. Rajavaram, H. Kim, C.H. Lee, W.S. Cho, C.H. Lee, and J. Lee: *Metall. Mater. Trans. B*, 2017, vol. 48B, pp. 1595–1601.
3. H. Kobatake, H. Khosroabadi, and H. Fukuyama: *Metall. Mater. Trans. A*, 2012, vol. 43A, pp. 2466–72.
4. A.K. Gangopadhyay, M.E. Blodgett, M.L. Johnson, A.J. Vogt, N.A. Mauro, and K.F. Kelton: *Appl. Phys. Lett.*, 2014, vol. 104, pp. 191907–11.
5. T. Ishikawa, J.T. Okada, P.F. Paradis, and Y. Watanabe: *J. Chem. Thermodyn.*, 2016, vol. 103, pp. 107–14.
6. M.P. SanSoucie, J.R. Rogers, V. Kumar, J. Rodriguez, X. Xiao, and D.M. Matson: *Int. J. Thermophys.*, 2016, vol. 37, pp. 76–86.
7. H.P. Wang, C.H. Zheng, P.F. Zou, S.J. Yang, L. Hu, and B. Wei: *J. Mater. Sci. Technol.*, 2017, vol. 34, pp. 436–39.
8. D.G. Quirinale, G.E. Rustan, S.R. Wilson, M.J. Kramer, A.I. Goldman, and M.I. Mendeleev: *J. Phys.: Condens. Matter*, 2015, vol. 27, pp. 085004–09.
9. A.K. Gangopadhyay, M.E. Blodgett, M.L. Johnson, J. McKnight, V. Wessels, A.J. Vogt, N.A. Mauro, J.C. Bendert, R. Soklaski, L.

- Yang, and K.F. Kelton: *J. Chem. Phys.*, 2014, vol. 140, pp. 044505–12.
10. I. Kaban, P. Jóvári, V. Kokotin, O. Shuleshova, B. Beuneu, K. Saksl, N. Mattern, J. Eckert, and A.L. Greer: *Acta Mater.*, 2013, vol. 61, pp. 2509–20.
 11. H.P. Wang and B. Wei: *Phys. Lett. A*, 2010, vol. 374, pp. 4787–92.
 12. H.L. Peng, T. Voigtmann, G. Kolland, H. Kobatake, and J. Brillo: *Phys. Rev. B*, 2015, vol. 92, pp. 4201–13.
 13. J. Brillo, A. Bytchkov, I. Egry, L. Hennem, G. Mathiak, I. Pozdnyakova, D.L. Price, D. Thiaudiere, and D. Zanghi: *J. Non-Cryst. Solids*, 2006, vol. 352, pp. 4008–12.
 14. J. Ding, Y.Q. Cheng, H. Sheng, and E. Ma: *Phys. Rev. B*, 2012, vol. 85, pp. 0201–05.
 15. C. Liang, H. Wang, J. Yang, B. Li, Y. Yang, and H. Li: *Appl. Surf. Sci.*, 2012, vol. 261, pp. 337–42.
 16. P. Sedmak, J. Pilch, L. Heller, J. Kopecek, J. Wright, P. Sedlak, M. Frost, and P. Sittner: *Science*, 2016, vol. 353, pp. 559–62.
 17. S. Kustov, D. Salas, E. Cesari, R. Santamarta, D. Mari, and J. Van Humbeeck: *Acta Mater.*, 2014, vol. 73, pp. 275–86.
 18. G. Fan, W. Chen, S. Yang, J. Zhu, X. Ren, and K. Otsuka: *Acta Mater.*, 2004, vol. 52, pp. 4351–62.
 19. B. Karbakhsh Ravari, S. Farjami, and M. Nishida: *Acta Mater.*, 2014, vol. 69, pp. 17–29.
 20. A.M. Pérez Sierra, J. Pons, R. Santamarta, I. Karaman, and R.D. Noebe: *Scripta Mater.*, 2016, vol. 124, pp. 47–50.
 21. R. Santamarta, R. Arróyave, J. Pons, A. Evirgen, I. Karaman, H.E. Karaca, and R.D. Noebe: *Acta Mater.*, 2013, vol. 61, pp. 6191–6206.
 22. N. Gao and W.S. Lai: *J. Phys.: Condens. Matter*, 2007, vol. 19, pp. 046213–24.
 23. J. Basu, B.S. Murty, and S. Ranganathan: *J. Alloy. Compd.*, 2008, vol. 465, pp. 163–72.
 24. L.C.R. Aliaga, M.F. de Oliveira, C. Bolfarini, W.J. Botta, and C.S. Kiminami: *J. Non-Cryst. Solids*, 2008, vol. 354, pp. 1932–35.
 25. P.F. Zou, H.P. Wang, S.J. Yang, L. Hu, and B. Wei: *Chem. Phys. Lett.*, 2017, vol. 681, pp. 101–04.
 26. M. Baskes: *Phys. Rev. B*, 1992, vol. 46, pp. 2727–42.
 27. W.S. Ko, B. Grabowski, and J. Neugebauer: *Phys. Rev. B*, 2015, vol. 92, pp. 4107–28.
 28. S. Plimpton: *J. Comput. Phys.*, 1995, vol. 117, pp. 1–19.
 29. H. Yoo, C. Park, S. Jeon, S. Lee, and G.W. Lee: *Metrologia*, 2015, vol. 52, pp. 677–84.
 30. T. Ishikawa, P.F. Paradis, and Y. Saita: *J. Jpn. Inst. Met.*, 2004, vol. 68, pp. 781–86.
 31. P.F. Paradis and W.K. Rhim: *J. Chem. Thermodyn.*, 1999, vol. 32, pp. 123–33.
 32. K.D. Machado, J.C. de Lima, C.E.M. de Campos, T.A. Grandi, and D.M. Trichês: *Phys. Rev. B*, 2002, vol. 66, pp. 4205–11.
 33. G.W. Lee, A.K. Gangopadhyay, R.W. Hyers, T.J. Rathz, J.R. Rogers, D.S. Robinson, A.I. Goldman, and K.F. Kelton: *Phys. Rev. B*, 2008, vol. 77, pp. 4102–09.